Combustion and Flame 211 (2020) 1–7

Contents lists available at ScienceDirect

Combustion and Flame

journal homepage: www.elsevier.com/locate/combustflame

Droplet combustion of kerosene augmented by stabilized nanoaluminum/oxidizer composite mesoparticles

Philip M. Guerieri[a], Rohit J. Jacob[a], Haiyang Wang[b], Dylan J. Kline[a,b], Michael R. Zachariah[b,*]

[a] University of Maryland, College Park, MD 20740, United States
[b] University of California, Riverside, CA 92506, United States

ARTICLE INFO

Article history:
Received 19 December 2018
Revised 28 January 2019
Accepted 21 July 2019
Available online 26 September 2019

Keywords:
Nanofuels
Electrospray
Droplet combustion
Nanoaluminum
Nanoenergetics
Liquid propellants

ABSTRACT

Inclusion of energetic and chemically active nanoparticles into liquid fuels and propellants is known to affect resultant combustion dynamics. Recently, the activity of such nanoparticle additives has been promoted using electrospray to preassemble said particles into nitrocellulose-bound mesoparticle (MP) clusters of either nanoaluminum (nAl) or oxygen-carrying nanoparticle primaries. In either case, stability in kerosene with TOPO surfactant and isolated droplet burning rates estimated in a free-droplet combustion experiment increase substantially with the MP additive architecture. Burning rates benefit from violent physical mixing of droplet systems which occurs when the carried nanoparticles are energetic and/or chemically active, causing gas generation, additive transport to the flame, energy or oxygen release, and further gas liberation accelerating the process. In this study, this same physical underlying mechanism is seen superimposed with the effects of another advantage of electrospray particle assembly: MP composition flexibility. By mixing nAl with oxide nanoparticles to form composite MPs, these novel additives for hydrocarbons are employed to modify kerosene and their effects are found to be dependent on the oxidizer chosen. Most notably, nAl/CuO MPs show evidence of interparticle thermite reaction in the droplet system yielding a cooperative benefit of the two constituents relative to either alone in MPs. Use of oxidizer co-additives and the MP architecture with nAl represents a flexible and promising method of overcoming low burning rates of hydrocarbons with high as-received nAl loadings and provides expansive means of tunability to tailor nanofuel properties.

1. Introduction

Augmentation of liquid propellants with energetic solids was proposed in the 1960's for increasing volumetric energy densities, but historically slurry-based fuels burned slowly and inefficiently due largely to agglomeration effects [1,2]. Since the operating envelope, capabilities, and performance of a vehicle can largely depend on the propulsion mode and energy source, promoting propellant energy density and combustion performance or flexibility can reap direct benefits for vehicle development [3,4]. Reducing the size scale of energetic solids to the nanoscale can increase reaction rate and shorten ignition delay, in addition to changing the agglomeration dynamics that previously plagued slurry fuels [2,5]. As such, numerous nanomaterials have been investigated in liquid fuels or propellants [3,4,6–17], including nanoaluminum (nAl) [6,7,11–13,18–24]. Agglomeration of solid additive particles remains an observed problem [22,24–28] but surfactants can be used to promote stabilization [5,7,10,20]. Evidence of gas release and physical disruption of droplets during combustion or "microexplosions" promoting burning rates and/or inhibiting agglomeration has been observed [10,20,28]. An interested reader is also directed to relevant reviews [1,5,29].

Previously we have demonstrated improved colloidal stability and significantly higher burning rate constants for nanofuels composed of both nanoaluminum [20] and oxygen-containing nanoparticles [10] when such additives are prepared for kerosene inclusion by electrospray assembly of so-called "mesoparticles" (MPs): nitrocellulose-bound nanoparticle clusters in the range of 1–5 μm in diameter. nAl in this configuration can increase energy density of kerosene by up to 8% with about 13 wt% solids loading [1]. Similar mechanisms were also identified for both classes of nanomaterial additives, namely that the marriage of chemical benefits of the additives (either energy density of nAl or oxygen release of oxidizers) with physical droplet disruptions caused by gas generation/eruptions during free-droplet combustion creates a positive feedback loop by way of eruptions releasing particles into

* Corresponding author.
E-mail address: mrz@engr.ucr.edu (M.R. Zachariah).

https://doi.org/10.1016/j.combustflame.2019.07.031
0010-2180/

the flame zone and subsequent acceleration of further disruptions [10,20]. While nAl represents added fuel density and is thought to increase the heat of combustion of the base fuel [20], oxidizer additives were hypothesized to improve diffusion-limited reaction kinetics because the most active candidates (e.g., KIO_4 and CuO) release gas-phase oxygen on the fuel-rich side of the droplet diffusion flame, causing faster fuel oxidation through vigorous physical mixing [10].

Considering the similar nature of the physical droplet disruption mechanisms of both nAl and oxidizer-based mesoparticle (MP) additives and their complementary chemical roles as fuel and oxidizer respectively, these two systems represent a prime opportunity to formulate composite particle additives with both solid fuel and oxidizer components. In this study, precursor suspensions containing nanoaluminum (nAl) and various oxidizer nanoparticles with colloidion nitrocellulose (NC) are electrosprayed to form composite NC-bound MPs which have previously exhibited improved combustion rates in dry powder experiments versus physically-mixed analogs [30–34]. These "thermite" MPs are added to kerosene and stabilized with trioctylphosphene oxide (TOPO) surfactant to assess effects on the free-droplet combustion by direct observation and estimation of burning rate constants relative to those of MPs with only nAl or oxidizers studied previously [10,20]. The role of the MP preassembly strategy is also evaluated for such thermite nanoparticle mixtures by comparing their activity in kerosene nanofuels with that of non-electrosprayed nanoparticles.

2. Experimental

2.1. Particle additives and nanofuel preparation

Energetic nanoparticles are prepared for kerosene (Sigma-Aldrich 329460, reagent grade) incorporation using electrospray to generate a cloud of volatile precursor solution droplets as described and first utilized for energetic nanoparticle modification by Wang et al. [32]. The precursor consists of a 3:1 mixture of ethanol and ether by volume with the particles of interest suspended by in-situ magnetic stirring within the syringe and NC binder in solution (5% NC binder by mass relative to nanoparticles). nAl, CuO, Al_2O_3, and MgO are purchased commercially as nanoparticles and utilized as-received (nAl: Novacentrix, Inc., 80% active Al with 2–5 nm oxide shell; CuO, MgO, and Al_2O_3: Sigma-Aldrich 544868, 549649, and 544833, respectively, with <50 nm particle size). KIO_4 (Sigma-Aldrich 210056) and ammonium perchlorate (AP, Sigma-Aldrich 208507) are purchased as solid powder reagents and are reformed into nanoparticles by spray drying aqueous solutions of each (4 mg/mL KIO_4 and 50 mg/mL AP) from a venturi-style collision atomizer through a silica desiccant diffusion dryer and into a tube furnace at 200 C for KIO_4 and 150 C for AP before collecting in an in-line 400 nm membrane filter [35]. Resulting KIO_4 and AP submicron particles are on the order of 0.1–1 μm primary particles in agglomerates of 0.5–10 μm. Stoichiometric mixtures of nAl and each oxidizer were added to the electrospray precursor solutions at 95 mg/mL (with 5 mg/mL of NC binder for a constant electrospray precursor solids loading of 100 mg/mL), sonicated for 1 h, and magnetically stirred overnight. Pumping the precursor though a probe needle charged to 10 kV situated 10 cm from a −10 kV aluminum foil substrate generates a cloud of precursor droplets as repulsive charge accumulation on the fluid overcomes surface tension and the cloud is electrostatically attracted to the substrate. Evaporation of the precursor solvent in-flight leaves the aggregated mesoparticles bound by precipitated NC binder which impinge on the foil substrate. Representative SEM images of nAl/oxidizer/NC MPs made for this study are shown in Fig. 1.

The electrosprayed MPs are added to kerosene in 0.3 mL batches at the concentrations shown in Table 1 with 50 mg/mL of TOPO surfactant (Sigma-Aldrich 223301) necessary to stabilize nAl and nAl MP nanofuels in kerosene. The surfactant loading is not varied with particle additive loading so as not to modify the combustion characteristics of the base kerosene/TOPO fuel. With MPs and TOPO added to the kerosene, the nanofuels are sonicated for 5 min and magnetically stirred 24 h before droplet combustion experiments are carried out. Qualitatively, stability of MP suspensions observed based on gravitational settling exceeded that of physical mixtures, but further work is necessary to consider their stability more formally. Concentration, composition, and morphology are likely contributing factors, but generally in this study MP suspensions appear stable longer than 12 h while physical mixtures noticeably settle in the order of minutes. Nanofuel particle loadings were based on equal nominal loadings of the nAl component and the appropriate oxidizer loading to comprise a stoichiometric mixture as determined by considering full conversion of the 80% active nAl to Al_2O_3 and kept just low enough to prevent capillary clogging of the nAl/CuO samples (which feature the highest mass loading). To compare each of these four loading levels to each other, data are plotted against "oxygen demand" referring to nAl loadings and/or "oxygen concentration" referring to an oxidizer loading. Physical mixtures were also formulated from the as-received commercial nAl with either CuO, MgO, or Al_2O_3 for comparison with their MP analogs by mixing of the nanoparticles with kerosene and TOPO in the same proportions as the MP nanofuels. Data plotted for oxidizer-only MPs are reproduced from [10] for all oxidizers except AP.

2.2. Free-droplet combustion characterization

Combustion of the nanofuels is studied utilizing a free-droplet burning apparatus in which droplets are ignited at the top of a 20 in. tall tower filled with oxygen as they fall past two methane igniter pilots, as described previously [10,20,36]. This experimental framework avoids the interference of a suspension filament used in stationary droplet burning experiments and facilitates estimation of a burning rate constant despite the presence of gas generation within droplets and disruptive gas eruption events common upon solid energetic addition which obscures the classical droplet diameter-based measurement of burning rate. This is accomplished by the approximation for the burning rate constant $K \cong D_0^2/t_{burn}$, recorded by one high-speed camera capturing the flame trace to measure burning time and another zoomed on the initially generated droplet to account for small variations in the size of each droplet formed by aerodynamic shedding from a vertical capillary (600 ± 50 μm), as depicted in Supplemental Information.

3. Results

Effects of thermite additives were assessed first by examining far-field color images of the burning droplets, shown as representative time-lapse images of a full droplet flame trace for each sample in Fig. 2, including those of oxide/NC MPs reproduced from a previous study [10] for comparison. It is noted that flame trace length alone is not a repeatable measure of burning rate due to varying falling velocities, and the details of later quantification of burning rate are available in previous publications [9,1,2]. Qualitatively, thermite MP additives cause similar droplet disruptions to both nAl/NC MPs and oxide/NC MPs characterized by stochastic expansions of the flames and ejected emitting particles. Each thermite type also appears similar to its respective oxide MP in general flame color and disruption timing with respect to the burning lifetime of the droplet. However, relative to either nAl or oxides alone in MPs, thermites feature larger amplitudes of the

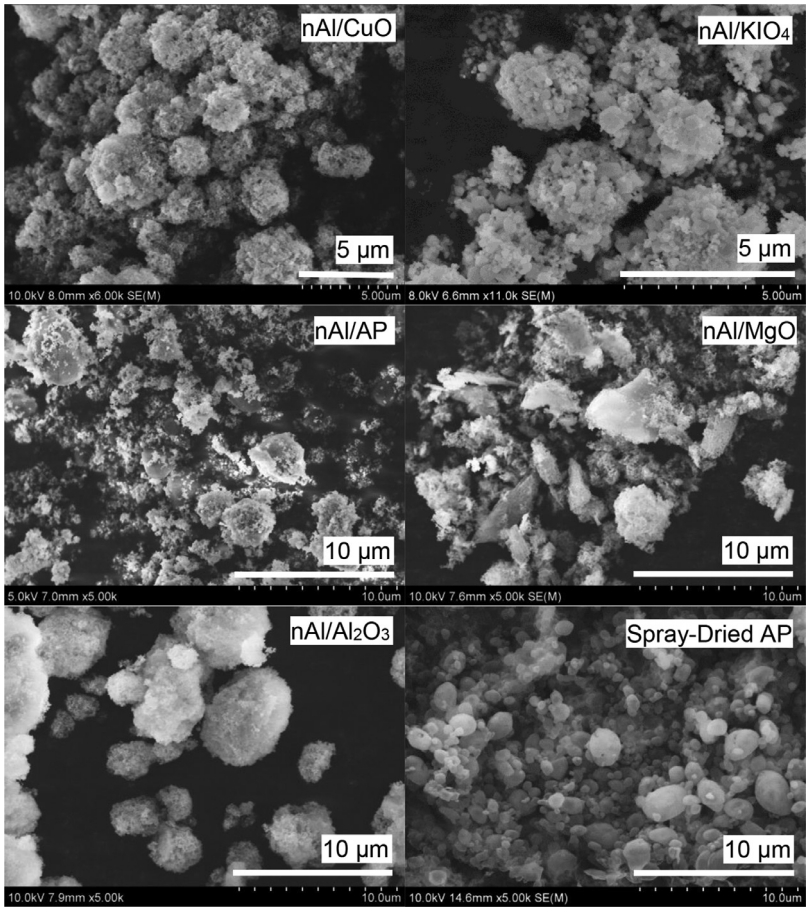

Fig. 1. SEM images of MP samples (with NC binder) collected from electrospray of nAl with various oxidizers.

Table 1
Sample compositions and loadings for nanofuels of nAl/Oxidizer/NC MPs, nAl/Oxidizer physical mixtures, and AP-only MPs or nanoparticles tested. (*nAl/NC data for AP, MgO, and Al_2O_3 was collected by testing a single 88% nAl + 12% NC by mass MP sample.)

	Solid Energetic Composition (wt%)		Nanofuel Solids Loading (wt%) Columns based on nominal nAl wt% of:			
	% nAl	% Ox	1.15	2.30	3.45	4.60
NC-bound MPs						
nAl/CuO/NC	21	74	5.6	10.6	15.0	19.1
nAl/KIO_4/NC	27	68	4.4	8.5	12.2	15.6
nAl/AP/NC	41	54	2.9	5.7	8.3	10.7
nAl/MgO/NC	34	61	3.5	6.8	9.8	12.7
nAl/Al_2O_3/NC	38	57	3.2	6.1	8.9	11.5
nAl/NC (for CuO)	81	0	1.5	3.0	4.4	5.8
nAl/NC (for KIO_4)	84	0	1.4	2.8	4.2	5.5
nAl/NC (for AP)*	89	0	1.4	2.7	4.0	5.3
nAl/NC (for MgO)*	87	0	1.4	2.8	4.1	5.4
nAl/NC (for Al_2O_3)*	88	0	1.4	2.7	4.0	5.3
AP/NC	0	92	1.7	3.4	5.0	6.6
Physical Mixtures						
nAl+CuO	22	78	5.3	10.1	14.4	18.3
nAl+MgO	36	64	3.3	6.5	9.4	12.1
nAl+AP	43	57	2.8	5.4	7.9	10.2
AP	0	100	1.6	3.1	4.6	6.1

flame expansions with disruptions and the added nAl is specifically responsible for more widespread brilliant white emission and more significant brilliant white termination bursts characteristic of aluminum combustion. Noted previously [10], CuO, KIO_4, and MgO are all active oxides which increase kerosene burning rates when added as MPs compared to adding the oxides as nanoparticles. Al_2O_3 MPs were observed to cause trivial effect as evident in its time-lapse, and AP MPs tested here in kerosene/TOPO also cause little droplet disruption. While the nanofuels of Al_2O_3 thermite MPs still appear to burn relatively slowly evidenced by the long flame trace, they do exhibit more emission flares and the nanofuels of nAl/AP MPs appear to burn significantly more disruptively than those of AP/NC MPs, more resembling nAl/NC MPs.

Burning rate constants estimated based on the generated droplet size and burning times of multiple droplets per sample

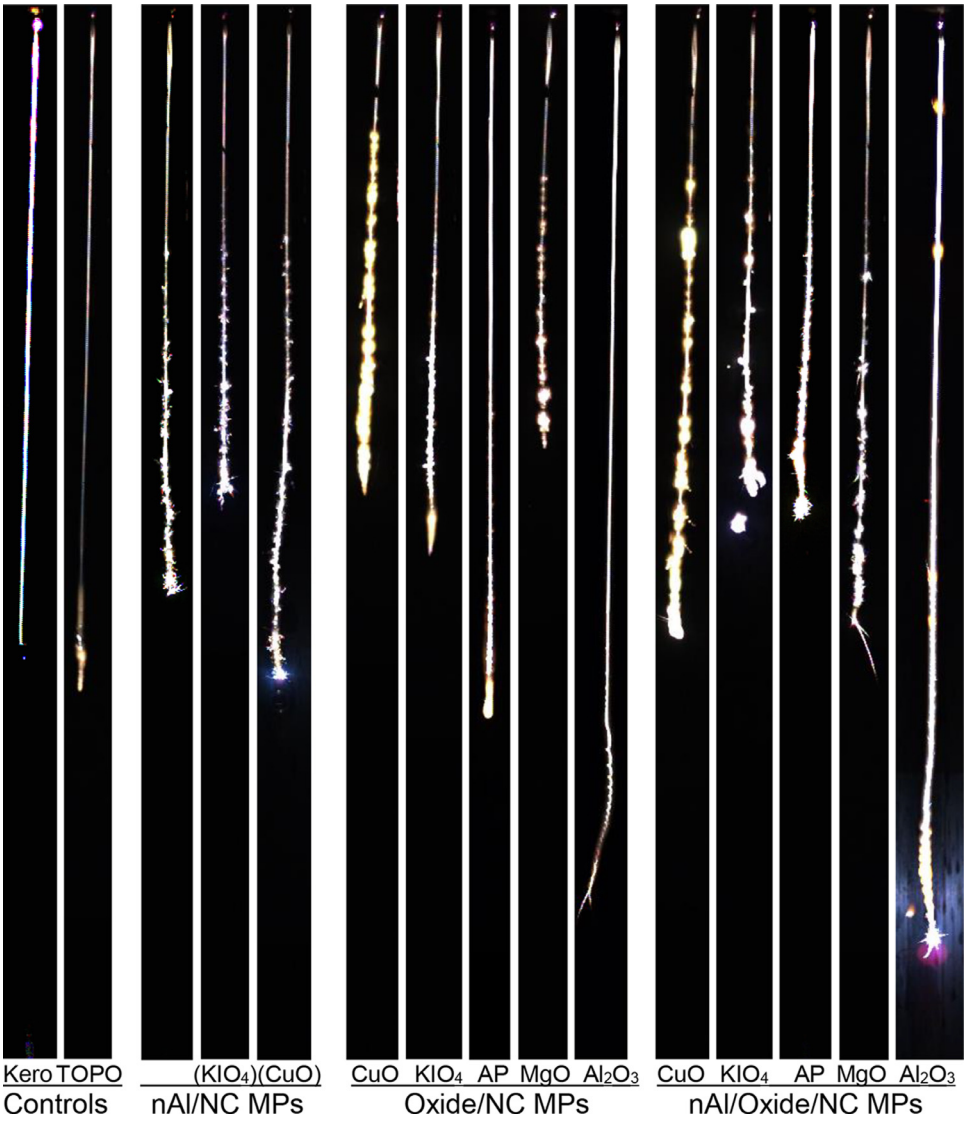

Fig. 2. Representative timelapse images of flame traces from nanofuels composed of various additive particle types including control samples (no particle additives), nAl/NC MPs and Oxide/NC MPs (from [10]) with NC% to match content in respective thermite MPs, and the nAl/oxidizer/5%NC Thermite MPs.

provide a more quantitative basis to compare effects of the various additives. Estimated burning rate constant changes compared to surfactant-only droplets are plotted in Fig. 3 relative to loading (on basis of oxygen concentration in the oxidizing particles, i.e., corresponding to the four columns of Table 1) and shown in two plots for illustration: one comparing all thermite MP samples, and another comparing MP samples to physically mixed samples (for CuO, MgO, and AP thermite systems). nAl/Al_2O_3 MPs in the highest loading level was not tested as it repeatedly clogged the sample delivery capillary. Overall, thermites of CuO and KIO_4 with nAl exhibited the highest burning rate increases which follows observations of oxide/NC MPs in [10]. nAl/AP additives showed a positive trend between loading and burning rate increase while nAl/MgO additives showed a generally negative trend and both burned slower than additives with CuO or KIO_4. Lastly, Al_2O_3 thermites have no discernible trend and hovered around zero-effect. For the three thermites tested as both MPs and physical mixtures, a primary finding of Guerieri et al. [10,20] is further supported: that the MP architecture facilitates significantly higher burning rates than unassembled particles added to kerosene with TOPO surfactant.

This data is further deconvoluted by considering the different oxidizers individually as shown in Fig. 4 for all except Al_2O_3 (shown in Supplemental Information to cause minimal change compared to control burning rates). CuO thermites burn faster than both nAl-only and CuO-only MPs suggesting that neither fuel nor oxidizer is individually dominant in the composite system and instead possibly feature a cooperative effect which follows from their common use as a nanothermite formulation. nAl/KIO_4 also constitutes an energetic nanothermite formulation [37,38], but nAl/KIO_4 nanofuels show burning rate constants overall similar to KIO_4-only MP nanofuels (with a slight but inconclusive benefit of the thermite at high loadings only). As opposed to the nAl/CuO thermite, this suggests that nAl and KIO_4 are not as inter-reactive during droplet combustion and instead the droplet burning is dominated by the activity of KIO_4. AP/NC MP nanofuels cause a relatively low burning rate increase around 10% which does not appear to scale with particle loading. The burning rate improvements are increased when nAl is added in the thermite MPs however both AP-containing MP additives cause lower burning rate increases than nAl/NC alone suggesting that the metal fuel is the beneficially active component which compensates for the less

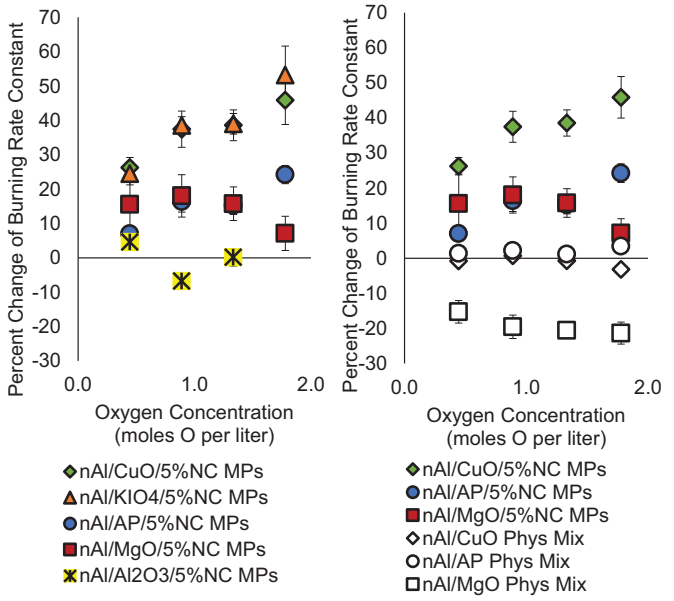

Fig. 3. Burning rate constants of nAl/Oxide/5%NC MPs of various oxide composition and comparison with physical mixtures. Represented as a percent-change of burning rate constant relative to surfactant-only kerosene/TOPO control. Filled markers indicate MP additives while hollow markers represent physical mixtures. Error bars depict one standard deviation in each direction.

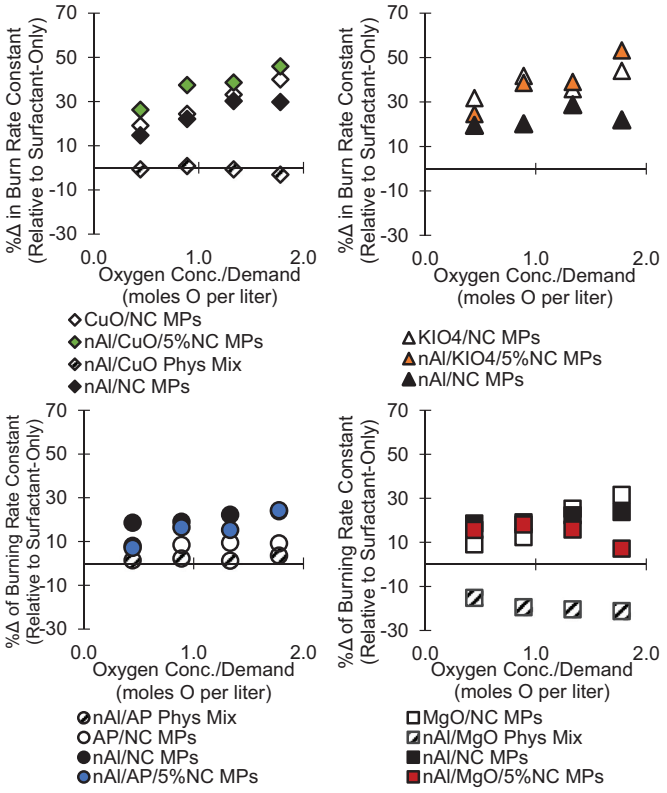

Fig. 4. Burning rate constants of various nanofuel types sorted by respective oxide composition with Oxide/NC MP data from [10] for comparison of MPs to physical mixtures. The four levels of "Oxygen Concentration/Demand" correspond to the four loading levels in Table 1.

active oxidizer particles. A contributing factor to the lower activity of AP compared to the other proven oxidizers, CuO and KIO_4, is its poor particle morphology, i.e., the significantly larger size of AP particles which decreases their interfacial contact with fuel species (evident in Fig. 1). MgO thermite MPs show a fourth possible effect: a negative relationship between nAl/MgO MP loading in the nanofuel and realized burning rate. MgO also features large particle sizes like AP, however, MgO is also not thermodynamically expected to react with the nAl fuel, unlike the other three oxidizers discussed above. As such, no possible exothermic interparticle reaction is present to compensate for lower mass diffusion rates caused by higher solid particle loadings and the MgO and nAl have a cooperatively negative effect on burning rate relative to either component alone in MPs.

4. Discussion

Overall, NC-bound MP mechanisms seen in [10,20] are reinforced by results herein, particularly regarding behavior caused by the nature of these composites preassembled with NC gas generator by electrospray. Based on time-lapse images of the droplet flames, most featured the expected gas release from the liquid droplet which perturbed the system, even with relatively inert MgO oxidizer and least so with fully inert Al_2O_3 oxide. This is theorized to be a physically disruptive characteristic of NC-bound MPs underlying the additives studied which can incite the first system perturbations/droplet disruptions as NC decomposes in and around the droplet, and increased physical mixing from these events can cause further NC decomposition and a self-acceleration of the process [20].

Differences in resultant burning rates and appearance of physical droplet disruptions among the various oxidizers alone [2] and among nAl thermites shows that the oxidizer particle characteristics play an important role in the gas-generation/disruption cycle. For these thermite nanofuels, further diagnostic information is required to observe the disruptions seen in the time-lapses in more detail and more confidently prove that the physical disruptions and nanoparticle chemical activity in the flame are strongly coupled causing this feedback loop. However, based on the prior oxidizer-only MP study and the burning rate measurements taken here, likely mechanisms of the different particle compositions can be supposed.

nAl/CuO thermite MPs most likely cause classical thermite intermetallic reaction between the Al and CuO upon ejection of the nanoparticles into the flame zone. Evidence from CuO-only MPs suggests the CuO particles survive passage to the flame zone before heating enough to decompose and release oxygen near 1000 K [10]. With the nanothermite ignition temperature of nAl/CuO also near 1000 K (ca. 1040 K [39]), initiation of the intermetallic reaction is also likely to take place once the particles reach the flame zone during a disruption. Rapid resulting energy release from the thermite reaction then constitutes a strong pathway to further disruption events. This mechanism is consistent with the cooperative effect of nAl and CuO loadings supposed previously from burning rates in this study. KIO_4 alternatively is thought to thermally decompose before it reaches the flame zone as it undergoes relatively low-rate heating (compared to faster heating if it reached the flame zone before decomposing) [10]. Therefore, nAl/KIO_4 thermite clusters are less likely to survive into the flame zone and reach their ignition temperature (ca. 950 K [37]) before the oxidizer has decomposed. The effect is therefore more likely a superposition of the increased combustion heat of nAl in the flame zone and KIO_4 oxygen release in the fuel-rich zone promoting diffusion-limited kinetics, although it is difficult to discern whether the possible intermetallic reaction can also be occurring to a lesser degree during disruptions. Both the CuO and KIO_4 thermite composite particles feature well-mixed small primary particles in the microscopy in Fig. 1 supporting the likelihood of intermetallic thermite reactions.

Microscopy in Fig. 1 shows that nAl/AP MP additives feature unfavorable morphologies with larger oxidizer primary particles

Table 2
Estimated reaction enthalpy change and Gibbs' Free Energy change for full Al oxidation to Al_2O_3 by CuO, MgO, or AP (calculated from heats of formation and standard enthalpies available in the NIST Webbook [40]).

Aluminum "Thermite" Reaction	ΔH_r (kJ/mol)	ΔG_r (kJ/mol)
$Al + 1.5\ CuO \rightarrow 0.5\ Al_2O_3 + 1.5\ Cu$	−601	−596
$Al + 1.5\ MgO \rightarrow 0.5\ Al_2O_3 + 1.5\ Mg$	67.5	65.7
$Al + 1.5\ NH4ClO4 \rightarrow 0.5\ Al_2O_3 + 1.5\ HCl + 0.75\ N_2 + 2.25\ H_2$	−759	−791

and therefore lower interfacial contact with nAl fuel. Wang et al. used alternate electrospray solvents to assemble nAl/AP/NC MPs wherein the AP instead dissolved into the precursor and thereby incorporated into the binder phase of the composite, which also featured higher NC loading (>17% instead of 5% by mass) [31], to overcome this otherwise poor microstructure. However, those particles were not colloidally stable in kerosene/TOPO when considered for this study and AP had to be added conventionally following electrospray procedures of the other thermites studied (also evidence that NC binder presence and characteristics significantly affect MP stability in kerosene/TOPO). Burning rate constants of the nAl/AP MP nanofuels are relatively poor and below those of nAl/NC MPs which dominate the burning rates at higher loadings, suggesting the rate increasing mechanism of nAl is the most active and that nAl/AP reaching the flame is very weak in accelerating gas generation and disruptions. While of nAl and AP is favorable (Table 2), kinetics will suffer from the poor microstructure. In addition, the simple stoichiometry considered ubiquitously for nAl/oxidizer compositions in this study (i.e., defined by full conversion of nAl to Al_2O_3) is not fitting for the complex AP oxidizer. NASA CEA calculation of equilibrium species from the Al/AP O/F ratio used herein (tabulated in Supporting information) suggests alternate products forming towards $AlCl_3$ instead of complete conversion of Al_2O_3 rendering the nAl/AP ratio used in this study more correctly classified as fuel-rich. The unique lack of a large termination burst in the time-lapse images supports the observation of significant particle transport into the flame at earlier times, possibly even due to added gas generation from the AP, but their non-ideal microstructure and mixture ratio limits the benefit of their early presence in the flame. While the nAl/AP system could be promising as liquid propellant additive, the greatest burning rate effects are evidently only realized with a proper marriage of appropriate physical disruption behavior and additive combustion performance, the latter of which is lacking for this additive.

nAl/MgO thermite MPs also have unfavorably large primary MgO particle morphology and therefore low interfacial contact with the nAl. They show decreasing burning rates with loading here suggesting that activity this additive in the flame zone hinders acceleration of the gas-generation/physical disruption feedback loop. Possible redox reactions involving the MgO surfaces in the flame zone [10] and nAl oxidation likely compete for thermal energy since an intermetallic reaction is not thermodynamically favorable between the two (Table 2), lessening the extent of either effect. Composite nAl/Al_2O_3 MPs used mainly as a control group here are unlikely to contribute any gas-generation to incite feedback, consistent with the largely null effect on burning rate observed.

Lastly, a loose correlation was observed between measured burning rate increases and energy release that would result from full redox of the nAl and oxidizer among the CuO, KIO_4, and MgO thermites, as plotted in Fig. 5 (excluding the AP thermite considering its poor microstructure and stoichiometry). The thermodynamic energy release is calculated based on the net enthalpy change from complete nAl oxidation to Al_2O_3 and metal oxide reduction to the base metal per volume of nanofuel. Since MgO is not thermodynamically favored to reduce to Mg by oxidation of Al, this case is merely hypothetical and constitutes a penalty applied to this additive for its competition between MgO and nAl for thermal energy (and surface reduced Mg versus nAl for oxygen). The relationship observed reinforces the supposition that combustion heat could be a method by which active particle additives promote or suppress the physical disruption feedback loop process to varying degrees. Namely, the additives most thermodynamically favored to release combustion heat inside the flame radius near the droplet are most likely to incite further disruptions, propagate the feedback loop, and thusly increase droplet burning rates. Further investigation including spectroscopic emission analysis or recovery and interrogation of combustion products could provide additional valuable evidence for more detail.

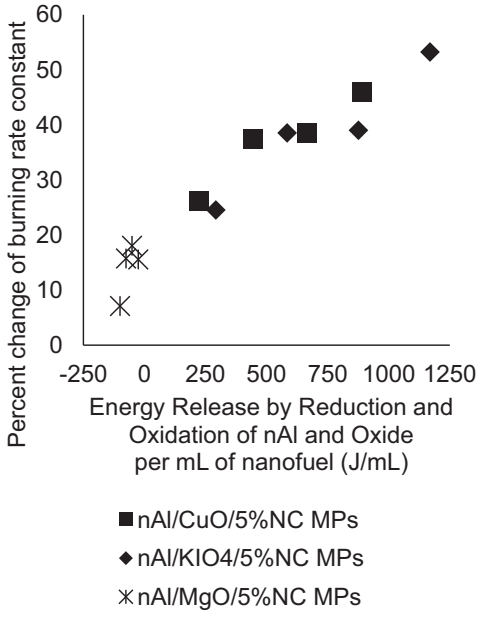

Fig. 5. Experimentally estimated burning rate constants of CuO, KIO_4, and MgO based thermite MPs with active oxides relative to theoretical enthalpy release of Al oxidation reaction by the particulate oxide.

5. Conclusions

Building upon prior work which identified significant modification of solid particle additive effects on kerosene with TOPO surfactant when said particles are preassembled into NC-bound MPs of nAl fuel [20] or various oxidizers [10], this study surveyed and investigated droplet combustion effects upon addition of nAl/oxidizer/5%NC thermite MPs to kerosene/TOPO to establish which composite compositions incited the most beneficial combustion effects and to probe the possible mechanisms of each formulation. A free-droplet combustion apparatus was employed to assess droplet burning rate constants with direct videography of burning droplet trajectories to qualify the disruptive combustion behavior. As expected, the most typically reactive and exothermic thermite MPs, those of nAl/CuO and nAl/KIO_4, exhibited the highest burning rate increases. Based on the observed activity of each thermite tested and mechanisms proposed, droplet burning rates

are thought to be increased most when the underlying physical disruption cycle facilitated by the NC-bound MP structure (caused by NC gas generation), cooperates with a chemical mechanism of the carried particle additive, whether that is highly exothermic intermetallic reaction (e.g., nAl/CuO), or relatively low temperature oxygen release (e.g., KIO_4). This coupling likely results in a self-accelerating pattern of gas generation, physical disruptions, particle liberation into the flame, heat or diffusion benefits from the additive, and further gas generation/disruptions: a powerful physical disruption feedback loop. Further detailed observations and diagnostics are necessary to confidently prove this coupling, and specifically probe for nAl fuel reaction upon droplet disruptions.

Acknowledgments

This work was made possible from the support of an Air Force Office of Scientific Research MURI grant and the Defense Threat Reduction Agency. SEM and TEM performed in the UMD AIMLab. Special thanks to Professor Richard Yetter of Penn State University for providing the original droplet combustion tower apparatus and to Haiyang Wang for inspiring and providing the spray-dried AP nanoparticles.

Supplementary materials

Supplementary material associated with this article can be found, in the online version, at doi:10.1016/j.combustflame.2019.07.031.

References

[1] P.R. Choudhury, Slurry fuels, Prog. Energy Combust. Sci. 18 (1992) 409–427.
[2] S.U.S. Choi, J.A. Eastman, Enhancing thermal conductivity of fluids with nanoparticles. 1995.
[3] J.L. Sabourin, R.A. Yetter, B.W. Asay, J.M. Lloyd, V.E. Sanders, G.A. Risha, et al., Effect of nano-aluminum and fumed silica particles on deflagration and detonation of nitromethane, Propellants Explos. Pyrotech. 34 (2009) 385–393, doi:10.1002/prep.200800106.
[4] J.L. Sabourin, D.M. Dabbs, R.A. Yetter, F.L. Dryer, I.A. Aksay, Functionalized graphene sheet colloids for enhanced fuel/propellant combustion, ACS Nano 3 (2009) 3945–3954, doi:10.1021/nn901006w.
[5] R.A. Yetter, G.A. Risha, S.F. Son, Metal particle combustion and nanotechnology, Proc. Combust. Inst. 32 (2009) 1819–1838, doi:10.1016/j.proci.2008.08.013.
[6] C. Allen, G. Mittal, C.J. Sung, E. Toulson, T Lee, An aerosol rapid compression machine for studying energetic-nanoparticle-enhanced combustion of liquid fuels, Proc. Combust. Inst. 33 (2011) 3367–3374, doi:10.1016/j.proci.2010.06.007.
[7] E. Xiu-tian-feng, X.M. Zhi, Y.M. Zhang, C.X. Li, J.J. Zou, X.W. Zhang, et al., Jet fuel containing ligand-protecting energetic nanoparticles: a case study of boron in JP-10, Chem. Eng. Sci. 129 (2015) 9–13, doi:10.1016/j.ces.2015.02.018.
[8] J.L. Sabourin, R.A. Yetter, V.S. Parimi, Exploring the effects of nanostructured particles on liquid nitromethane combustion, J. Propuls. Power 26 (2010) 1006–1015, doi:10.2514/1.48579.
[9] K.W. McCown, E.L. Petersen, Effects of nano-scale additives on the linear burning rate of nitromethane, Combust. Flame 161 (2014) 1935–1943, doi:10.1016/j.combustflame.2013.12.019.
[10] P.M. Guerieri, R.J. Jacob, J.B. DeLisio, M.C. Rehwoldt, M.R. Zachariah, Stabilized microparticle aggregates of oxygen-containing nanoparticles in kerosene for enhanced droplet combustion, Combust. Flame 187 (2018) 77–86, doi:10.1016/j.combustflame.2017.08.026.
[11] M.J. Kao, C.C. Ting, B.F. Lin, T.T. Tsung, Aqueous aluminum nanofluid combustion in diesel fuel, J. Test Eval. 36 (2008) 186–190.
[12] H. Tyagi, P.E. Phelan, R. Prasher, R. Peck, T. Lee, J.R. Pacheco, et al., Increased hot-plate ignition probability for nanoparticle-laden diesel fuel, Nano Lett. (2008), doi:10.1021/nl080277d.
[13] R.N. Mehta, M. Chakraborty, P.A. Parikh, Nanofuels: combustion, engine performance and emissions, Fuel 120 (2014) 91–97, doi:10.1016/j.fuel.2013.12.008.
[14] V. Sajith, C.B. Sobhan, G.P. Peterson, Experimental investigations on the effects of cerium oxide nanoparticle fuel additives on biodiesel, Adv. Mech. Eng. (2010), doi:10.1155/2010/581407.
[15] N.S. Sarvestany, A. Farzad, E. Ebrahimnia-Bajestan, M. Mir, Effects of magnetic nanofluid fuel combustion on the performance and emission characteristics, J. Dispers. Sci. Technol. 35 (2014) 1745–1750, doi:10.1080/01932691.2013.874296.
[16] N. Singh, R.S. Bharj, Effect of CNT-Emulsified fuel on performance emission and combustion characteristics of four stroke diesel engine, Int. J. Curr. Eng. Technol. 5 (2015) 477–485.
[17] B. Van Devener, S.L. Anderson, Breakdown and combustion of JP-10 fuel catalyzed by nanoparticulate CeO_2 and Fe_2O_3, Energy Fuels 20 (2006) 1886–1894, doi:10.1021/ef060064g.
[18] I. Javed, S.W. Baek, K. Waheed, Autoignition and combustion characteristics of heptane droplets with the addition of aluminium nanoparticles at elevated temperatures, Combust. Flame 162 (2015) 191–206, doi:10.1016/j.combustflame.2014.07.015.
[19] S. Tanvir, L. Qiao, Effect of addition of energetic nanoparticles on droplet-burning rate of liquid fuels, J. Propuls. Power 31 (2015) 408–415, doi:10.2514/1.B35500.
[20] P.M. Guerieri, J.B. DeLisio, M.R. Zachariah, Nanoaluminum/nitrocellulose microparticle additive for burn enhancement of liquid fuels, Combust. Flame 176 (2017) 220–228, doi:10.1016/j.combustflame.2016.10.011.
[21] Y.A. Gan, L. Qiao, Optical properties and radiation-enhanced evaporation of nanofluid fuels containing carbon-based nanostructures, Energy Fuels 26 (2012) 4224–4230, doi:10.1021/ef300493m.
[22] Y.N. Gan, L. Qiao, Radiation-enhanced evaporation of ethanol fuel containing suspended metal nanoparticles, Int. J. Heat Mass Transf. 55 (2012) 5777–5782, doi:10.1016/j.ijheatmasstransfer.2012.05.074.
[23] I. Javed, S.W. Baek, K. Waheed, G. Ali, S.O. Cho, Evaporation characteristics of kerosene droplets with dilute concentrations of ligand-protected aluminum nanoparticles at elevated temperatures, Combust. Flame 160 (2013) 2955–2963, doi:10.1016/j.combustflame.2013.07.007.
[24] I. Javed, S.W. Baek, K. Waheed, Effects of dense concentrations of aluminum nanoparticles on the evaporation behavior of kerosene droplet at elevated temperatures: the phenomenon of microexplosion, Exp. Therm. Fluid Sci. 56 (2014) 33–44.
[25] I. Javed, S.W. Baek, K. Waheed, Evaporation characteristics of heptane droplets with the addition of aluminum nanoparticles at elevated temperatures, Combust. Flame 160 (2013) 170–183, doi:10.1016/j.combustflame.2012.09.005.
[26] Y. Gan, L. Qiao, Evaporation characteristics of fuel droplets with the addition of nanoparticles under natural and forced convections, Int. J. Heat Mass Transf. 54 (2011) 4913–4922.
[27] Y.A. Gan, Y.S. Lim, L. Qiao, Combustion of nanofluid fuels with the addition of boron and iron particles at dilute and dense concentrations, Combust. Flame 159 (2012) 1732–1740, doi:10.1016/j.combustflame.2011.12.008.
[28] A. Miglani, S. Basu, Coupled mechanisms of precipitation and atomization in burning nanofluid fuel droplets, Sci. Rep. 5 (2015), doi:10.1038/srep15008.
[29] D. Sundaram, V. Yang, R.A. Yetter, Metal-based nanoenergetic materials: synthesis, properties, and applications, Prog. Energy Combust. Sci. 61 (2017) 293–365, doi:10.1016/j.pecs.2017.02.002.
[30] H.Y. Wang, J.B. DeLisio, G.Q. Jian, W.B. Zhou, M.R. Zachariah, Electrospray formation and combustion characteristics of iodine-containing Al/CuO nanothermite microparticles, Combust. Flame 162 (2015) 2823–2829, doi:10.1016/j.combustflame.2015.04.005.
[31] H.Y. Wang, R.J. Jacob, J.B. DeLisio, M.R. Zachariah, Assembly and encapsulation of aluminum NP's within AP/NC matrix and their reactive properties, Combust. Flame 180 (2017) 175–183, doi:10.1016/j.combustflame.2017.02.036.
[32] H.Y. Wang, G.Q. Jian, S. Yan, J.B. DeLisio, C. Huang, M.R. Zachariah, Electrospray formation of gelled nano-aluminum microspheres with superior reactivity, ACS Appl. Mater. Interfaces 5 (2013) 6797–6801, doi:10.1021/am401238t.
[33] G. Young, H.Y. Wang, M.R. Zachariah, Application of nano-aluminum/nitrocellulose mesoparticles in composite solid rocket propellants, Propellants Explos. Pyrotech. 40 (2015) 413–418, doi:10.1002/prep.201500020.
[34] R.J. Jacob, B.R. Wei, M.R. Zachariah, Quantifying the enhanced combustion characteristics of electrospray assembled aluminum mesoparticles, Combust. Flame 167 (2016) 472–480, doi:10.1016/j.combustflame.2015.09.032.
[35] K. Okuyama, I.W. Lenggoro, Preparation of nanoparticles via spray route, Chem. Eng. Sci. 58 (2003) 537–547, doi:10.1016/S0009-2509(02)00578-X.
[36] P.M. Guerieri, S. DeCarlo, B. Eichhorn, T. Connell, R.A. Yetter, X. Tang, et al., Molecular aluminum additive for burn enhancement of hydrocarbon fuels, J. Phys. Chem. A 119 (2015) 11084–11093, doi:10.1021/acs.jpca.5b08580.
[37] G.Q. Jian, J.Y. Feng, R.J. Jacob, G.C. Egan, M.R. Zachariah, Super-reactive nanoenergetic gas generators based on periodate salts, Angew. Chem.-Int. Ed. 52 (2013) 9743–9746, doi:10.1002/anie.201303545.
[38] W.B. Zhou, J.B. DeLisio, X.Z. Wang, M.R. Zachariah, Reaction mechanisms of potassium oxysalts based energetic composites, Combust. Flame 177 (2017) 1–9, doi:10.1016/j.combustflame.2016.05.024.
[39] G. Jian, S. Chowdhury, K. Sullivan, M.R. Zachariah, Nanothermite reactions: is gas phase oxygen generation from the oxygen carrier an essential prerequisite to ignition? Combust. Flame 160 (2013) 432–437, doi:10.1016/j.combustflame.2012.09.009.
[40] P.J. Linstrom, W.G. Mallard, The NIST chemistry WebBook: a chemical data resource on the internet, J. Chem. Eng. Data 46 (2001) 1059–1063, doi:10.1021/je000236i.